

Factorized Video Autoencoders for Efficient Generative Modelling

Mohammed Suhail¹

suhailmhd@google.com

Carlos Esteves¹

machc@google.com

Leonid Sigal^{2,3,4}

lsigal@cs.ubc.ca

Ameesh Makadia¹

makadia@google.com

¹Google²University of British Columbia³Vector Institute for AI⁴Canada CIFAR AI Chair

Abstract

Latent variable generative models have emerged as powerful tools for generative tasks including image and video synthesis. These models are enabled by pretrained autoencoders that map high resolution data into a compressed lower dimensional latent space, where the generative models can subsequently be developed while requiring fewer computational resources. Despite their effectiveness, the direct application of latent variable models to higher dimensional domains such as videos continues to pose challenges for efficient training and inference. In this paper, we propose an autoencoder that projects volumetric data onto a four-plane factorized latent space that grows sublinearly with the input size, making it ideal for higher dimensional data like videos. The design of our factorized model supports straightforward adoption in a number of conditional generation tasks with latent diffusion models (LDMs), such as class-conditional generation, frame prediction, and video interpolation. Our results show that the proposed four-plane latent space retains a rich representation needed for high-fidelity reconstructions despite the heavy compression, while simultaneously enabling LDMs to operate with significant improvements in speed and memory.

1. Introduction

A defining trait of recent advances in image and video generation is that, as models grow more powerful, they increasingly push against the boundaries of current computational limits. Despite their impressive generative capabilities, these models' vast resource demands hinder scalability and discourage widespread deployment. Naturally, improving the efficiency of these generative models has become an active research concern [1, 19, 60, 61].

One effective strategy to make generative modeling computationally feasible is through latent modeling [1, 3, 5, 10, 17, 19, 37, 38, 41]. By compressing high-resolution visual data into a compact latent space, latent models significantly reduce the computational burden for generative mod-

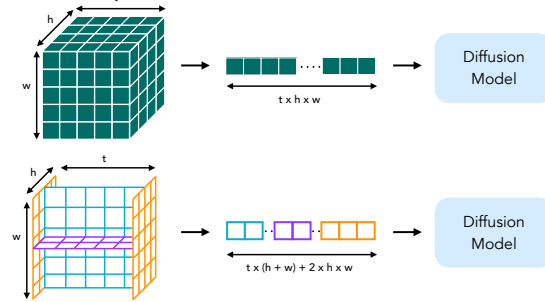


Figure 1. **Factorized latent representation.** Traditional volumetric latents in diffusion models yield a sequence length of $t \times h \times w$ (top row), which scales linearly with the input size and demands high computational resources. Our proposed factorized representation reduces sequence length to $t \times (h + w) + 2 \times h \times w$ (bottom row), achieving a more compact latent space that scales sublinearly with input size, enabling faster, more efficient video generation without sacrificing quality.

els. However, in typical latent model autoencoders, the resulting embedding size still scales linearly with the original input size, so this compression offers only a limited benefit when deployed in very high dimensional domains, such as videos [19, 38] (see Figure 1).

In this paper, we explore improving the efficiency of latent generative models through more aggressive reduction of the latent resolution. The central objective is to achieve this compression without sacrificing representation quality. To address this challenge, we propose a novel *four-plane factorized latent autoencoder* that maps volumetric space-time signals onto a latent space through four axis-aligned planar projections. Since the orthogonal projections capture complementary features of the space-time volume, the original signal can still be reconstructed from this more compact latent space with high fidelity. We summarize the key attributes of our contribution below:

- *Compact yet expressive factorization:* four-plane factorization significantly compresses volumetric latent embeddings, scaling sublinearly with the total input size

(see Fig. 1). Despite this compression, it retains high-fidelity reconstructions.

- *Faster generation without sacrificing quality*: we demonstrate the factorized latent space is suitable for high quality generative modeling. A conventional transformer-based diffusion model trained to generate factorized latents is twice as fast compared to producing volumetric features [19].
- *Versatility for image-conditioned tasks*: our experiments show how the four-plane structure seamlessly accommodates a variety of applications such as two-frame interpolation and future frame prediction.

Across a variety of tasks, our experiments suggest the proposed four-plane factorized autoencoder provides an efficient alternative for generative models that traditionally operate on volumetric latent spaces.

2. Related work

2.1. Diffusion models for video synthesis

Denoising Diffusion Probabilistic Models (DDPM) [21] introduced a novel method for generating images by iteratively denoising a sequence of noisy images. This approach has been highly successful for both image [10, 12, 24, 37, 43] and video synthesis [3, 4, 18, 22, 23, 53].

Of the more recent diffusion models developed for video generation, many operate on a volumetric spatiotemporal latent space. VDM [23] employs a 3D U-Net autoencoder architecture [9, 42] to learn this space. To address scalability for high resolution video generation, Imagen Video [22] extends VDM by introducing a cascade of models that essentially alternate temporal and spatial superresolution. Lumière [2] introduced the STUNet architecture, which generates entire videos directly with improved temporal coherence. VideoLDM [4] constructs a video model starting with pretrained image models and inserting temporal layers before fine-tuning on high-quality videos.

2.2. Video tokenizers

Many of the latent video diffusion models highlighted above rely on some form of video tokenization [15, 19, 52, 55, 62] to compress high dimensional videos into a compact latent space. The pioneering vector quantization approaches for image tokenization, for example VQ-VAE [49], VQ-VAE2 [39], and VQGAN [14], can be applied to videos in a frame-by-frame manner. MAGVIT [56] introduced a 3D-VQ autoencoder to quantize video data into spatio-temporal tokens, making it a powerful tool for a range of video generation tasks such as a frame prediction, video inpainting, and frame interpolation. MAGVIT-v2 [57] introduced significant advancements, including a lookup-free quantization method, which allows for an expanded vocabulary without compromising performance. Additionally, MAGVIT-v2 en-

ables joint image and video modeling through a causal 3D CNN architecture. The MAGVIT-v2 tokenizer was used successfully in W.A.L.T [19] for photorealistic image and video generation. The early 3D encoder layers in our factorized architecture are based on MAGVIT-v2.

2.3. Video frame interpolation

Video frame interpolation [13, 29] has distinct interpretations depending on the temporal distance between frames. In case with significant motion between frames, the challenging task can be addressed by generative models. The application of our factorized latent representation to frame interpolation can be categorized as a two-frame conditioned diffusion model. The first such effort to use a latent diffusion model was LDMVFI [11]. In contrast, VIDIM [27] models in pixel space and generates the entire video at once improving temporal consistency. To improve quality, VIDIM employs a cascaded diffusion approach: it first generates a low-resolution video, followed by an upsampling diffusion model that refines the output to higher resolutions

2.4. Tri-plane factorization

Tri-plane representations, which factorize volumetric data into three orthogonal 2D planes, have been widely used as compact representations of 3D neural fields [7, 16, 45]. Coupled with diffusion model architectures suited to planar representations, they have been used for a variety of applications, such as textured 3D model generation [54], 3D neural field generation [45], and semantic scene generation [32]. The same concept was applied to videos in PVDM [59], where encoding videos to tri-plane latent features enables the use of a 2D U-Net architecture [12] for training diffusion models, bringing significant improvements in efficiency. However, tri-plane approaches are still quite far behind their volumetric counterparts in generation quality, and the tri-plane representation cannot support different use cases. Both of these points are addressed by our distinctive four-plane factorization.

3. Factorized video latent representations

In latent video diffusion models, a key component is the autoencoder, which compresses the input video data into a compact latent representation. To achieve this, prior works [19, 20] employ a 3D convolutional architecture that encodes the 3D video volume $\mathbf{X} \in \mathbb{R}^{T \times H \times W \times C}$ into a feature volume $\mathbf{Z} \in \mathbb{R}^{t \times h \times w \times c}$, where $t = \frac{T}{f_t}$, $h = \frac{H}{f_s}$, $w = \frac{W}{f_s}$. Here f_t and f_s are the temporal and spatial down-sampling factors. The channel dimension c is typically expanded (e.g., $c = 8$ is a common choice that balances autoencoder reconstruction and diffusion performance).

While this compression does offer significant reduction in the spatial and temporal resolution, the total size $(t \times h \times$

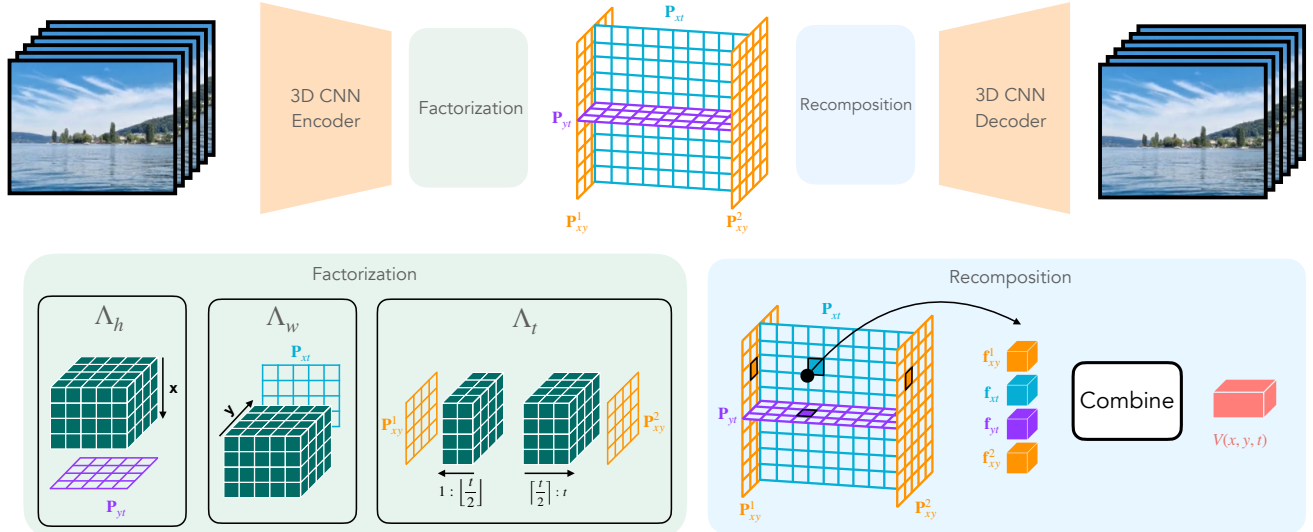


Figure 2. **Model overview.** The autoencoder first maps the input video into a volumetric latent representation through 3D convolutional architecture, which is then factorized into four planes. Temporal planes are created by mean pooling along the height and width dimensions, capturing time-varying features. Spatial planes are obtained by splitting along the time axis and independently averaging along this dimension, focusing on spatial consistency (highlighted in green). During decoding, the four planes are mapped back into a volume: for each spatial-temporal location, features from the corresponding four planes (highlighted in blue) are concatenated to reconstruct the full volumetric features. These combined features are passed through a decoder to produce the final output video.

w) still scales linearly with the input size. For computationally expensive generative models such as transformer [50]-based diffusion models, this sequence length would still pose a challenge. Improving the efficiency of transformer-based models can either be achieved by addressing the design of the model itself (*e.g.*, sub-quadratic attention mechanisms), or by decreasing the sequence length. In this work we explore the latter by introducing a four-plane factorized autoencoder that we describe in the following section.

3.1. Four plane factorization

Our approach provides a direct and effective solution to reducing the cubic complexity of volumetric spatiotemporal latent spaces. By decomposing the 3D feature volume into four complementary planes, our method captures rich spatial and temporal structures while significantly improving efficiency. This streamlined representation not only accelerates training and inference but also reduces memory overhead without compromising reconstruction quality. Beyond efficiency gains, the four-plane factorization introduces a versatile framework adaptable to a wide range of video generation tasks, including class-conditional generation, frame extrapolation, and video interpolation.

3.1.1. Factorization.

Given an input video $\mathbf{X} \in \mathbb{R}^{T \times H \times W \times 3}$, our encoder network first converts it into a feature volume $\mathbf{Z} \in \mathbb{R}^{t \times h \times w \times c}$ using a causal 3D convolution architecture similar to the one introduced in MAGVIT-v2 [58]. The feature volume is then factorized into four planes along three directions: two spatial planes, $\mathbf{P}_{xy}^1, \mathbf{P}_{xy}^2 \in \mathbb{R}^{h \times w \times c}$, aligned along the xy -dimension, and two spatiotemporal planes, $\mathbf{P}_{xt} \in \mathbb{R}^{t \times h \times c}$ and $\mathbf{P}_{yt} \in \mathbb{R}^{t \times w \times c}$, aligned along the xt and yt dimensions, respectively. The two spatio-temporal planes \mathbf{P}_{xt} and \mathbf{P}_{yt} are obtained by collapsing the height and width dimensions, respectively:

$$\mathbf{P}_{xt} = \Lambda_w(\mathbf{Z}) \in \mathbb{R}^{t \times h \times c} \quad (1)$$

$$\mathbf{P}_{yt} = \Lambda_h(\mathbf{Z}) \in \mathbb{R}^{t \times w \times c} \quad (2)$$

where Λ_h and Λ_w performs pooling or dimensionality reduction operation along the required dimensions.

The spatial planes \mathbf{P}_{xy}^1 and \mathbf{P}_{xy}^2 contain the temporally aggregated features across frames, capturing the spatial structure and background information in the video. We adapt our factorization approach based on the application. For class-conditional generation and frame prediction, we split the latent feature volume $\mathbf{Z} \in \mathbb{R}^{t \times h \times w \times c}$ into two segments along the temporal dimension, then aggregate each

segment over T , yielding:

$$\mathbf{P}_{xy}^1 = \Lambda_t(\mathbf{Z}_{1:\lfloor \frac{t}{2} \rfloor}), \quad \mathbf{P}_{xy}^2 = \Lambda_t(\mathbf{Z}_{\lceil \frac{t}{2} \rceil:t}), \quad (3)$$

where Λ_t is an aggregation function similar to $\Lambda_{h,w}$, $\lfloor \cdot \rfloor$ and $\lceil \cdot \rceil$ represents the floor and ceil function respectively.

For the interpolation task only the first and last frames are available at inference and therefore the spatial plane cannot contain information from other timesteps. To address this, we obtain the spatial planes by encoding only the first and last frames using our encoder. Specifically, we set:

$$\mathbf{P}_{xy}^1 = E(\mathbf{X}_0), \quad \mathbf{P}_{xy}^2 = E(\mathbf{X}_T), \quad (4)$$

where E denotes our video encoder and \mathbf{X}_0 and \mathbf{X}_T are the boundary frames. Since our model uses a 3D CNN with causal temporal padding, it can naturally encode images without requiring additional modifications. This approach effectively incorporates key frame information into the spatial planes, enhancing the model’s interpolation accuracy.

3.1.2. Recomposition

Given the four latent planes \mathbf{P}_{xy}^1 , \mathbf{P}_{xy}^2 , \mathbf{P}_{xt} , and \mathbf{P}_{yt} , the decoder reconstructs the input video by first reconstituting these planes back into a 3D feature volume. To utilize existing 3D convolutional architectures, we construct an intermediate volume $\mathbf{V} \in \mathbb{R}^{t \times h \times w \times c}$ by back-projecting features from each plane onto corresponding locations within the target volume dimensions (t, h, w) .

For any spatial-temporal location (x, y, t) in the volume, we extract features from each of the planes by projecting onto their respective dimensions (depicted in the blue box in Figure 2). Specifically:

$$\begin{aligned} \mathbf{f}_{xy}^1 &= \mathbf{P}_{xy}^1(x, y), & \mathbf{f}_{xy}^2 &= \mathbf{P}_{xy}^2(x, y) \\ \mathbf{f}_{xt} &= \mathbf{P}_{xt}(x, t), & \mathbf{f}_{yt} &= \mathbf{P}_{yt}(y, t). \end{aligned}$$

Here \mathbf{f}_{xy}^1 , \mathbf{f}_{xy}^2 , \mathbf{f}_{xt} , and \mathbf{f}_{yt} will contain features queried from their respective planes, using the corresponding spatial or temporal coordinates. These features are then combined using an operation such as element-wise addition or concatenation, yielding:

$$\mathbf{V}(x, y, t) = \text{Combine}(\mathbf{f}_{xy}^1, \mathbf{f}_{xy}^2, \mathbf{f}_{xt}, \mathbf{f}_{yt}),$$

where Combine represents the recomposition operation, e.g., summation or concatenation, along the channel dimension.

The reconstructed feature volume \mathbf{V} is then fed into a decoder with a structure similar to MAGVIT-v2, which progressively upsamples the features and applies 3D convolutions to generate the final video $\hat{\mathbf{X}} \in \mathbb{R}^{T \times H \times W \times 3}$.

3.2. Generative modeling with factorized latents

With a trained factorized latent model, we obtain a compact, efficient representation of input video data, suitable for training generative models. In our experiments we utilize established techniques for transformer-based latent diffusion models.

Latent diffusion models (LDMs) gradually transform the latent representation of data into noise in a forward diffusion process, then reverse this transformation to generate new samples. Given an initial latent sample \mathbf{x}_0 , the forward process generates a sequence of increasingly noisy latents $\{\mathbf{z}_t\}_{t=1}^T$ as $\mathbf{z}_t = \sqrt{\alpha_t} \mathbf{z}_{t-1} + \sqrt{1 - \alpha_t} \epsilon$, $\mathbf{x}_0 \approx D(\mathbf{z}_0)$ where α_t controls the noise schedule and D decodes the final latent back to data space. The reverse process, defined by $p_\theta(\mathbf{z}_{t-1} | \mathbf{z}_t) = \mathcal{N}(\mathbf{z}_{t-1}; \mu_\theta(\mathbf{z}_t, t), \sigma_t^2 \mathbf{I})$, seeks to denoise the latent variables and reconstruct the original data distribution. This denoising is learned by minimizing a variational lower bound, often simplified into practical objectives [21]. Here, we adopt the v-parameterization, following recent diffusion improvements [44].

To train a LDM on our factorized representation we use a transformer architecture. We create a 1D sequence by flattening the four planes— \mathbf{P}_{xt} , \mathbf{P}_{yt} , \mathbf{P}_{xy}^1 , and \mathbf{P}_{xy}^2 —and concatenating them along the sequence length dimension. This results in a sequence length of $h \times t + w \times t + 2 \times h \times w$ (as shown in Figure 1).

4. Experiments

The focus of our experiments is to show that the four-plane factorized model can generally and seamlessly replace volumetric latent spaces when modeling videos. To understand the model’s representation capability, we will quantify the compression versus reconstruction tradeoff (Sec. 4.1). To demonstrate its widespread applicability, we deploy the factorized latent space in varied generative tasks such as class-conditional video generation (Sec. 4.2), future frames prediction (Sec. 4.3), and two-frame interpolation (Sec. 4.4). Notably, the factorized autoencoder design is used without modification across experiments, as only the training data changes to ensure fair comparisons for each task.

4.1. Autoencoder reconstruction

One primary consideration of the proposed factorization is if the considerable latent compression comes at a cost in representation quality. For this, we compare the reconstructions from a baseline volumetric autoencoder against our factorized approach. The factorized encoder and decoder share the same architecture as the volumetric baseline, differing only in the factorization and recomposition steps. Specifically, to obtain the planes from the latent feature volume, we use average pooling as the factorization operations Λ_h , Λ_w and Λ_t . To recompose the planes into feature

volume, we use the concatenation operation as Combine. We discuss further architecture and training details in the appendix.

We chose the W.A.L.T. [19] autoencoder as our volumetric baseline model as it has shown state of the art performance on multiple benchmark tasks such as class-conditional video generation and frame extrapolation. Furthermore we were able to reproduce the model in terms of similar datasets and performance, allowing us to evaluate it in new settings as well.

We trained the volumetric and our four-plane factorized model on the Kinetics-600 (K600) [6] dataset, consisting of nearly 400,000 video clips, covering around 600 action classes and exhibiting a wide range of human activities. Tab. 1 shows the reconstruction quality for 128×128 resolution videos is nearly identical for both the volumetric and factorized autoencoders, while the latent size (sequence length) is nearly halved for the factorized. We also train a 256×256 model by attaching an extra layer to the encoder and decoder architecture (see appendix for details), leaving the latent size unchanged and observe comparable performance for the volumetric and fourplane autoencoder.

Whereas W.A.L.T. adopts a continuous autoencoder framework, some recent works for latent video generation have opted for a variational autoencoder (VAE [31]) design [52, 55, 62]. Our factorized proposal is not predicated on this decision, so we would expect similar conclusions for our approach in the VAE setting. To validate this, we conduct two additional experiments. First, we modify W.A.L.T. autoencoder to incorporate a VAE decoder and construct a corresponding factorized-VAE variant. Second, we adopt WF-VAE [34] from OpenSoraPlan [35], training the VAE using our factorized representation and comparing its performance against the baseline. For experiments with the W.A.L.T. autoencoder, we use a latent dimensionality of 8, while for WF-VAE, we set the latent dimensionality to 4. Table 1 confirms the relative performance holds across both VAE and AE settings. Since W.A.L.T. (AE) is the established baseline, our subsequent evaluations are all performed in the AE setting.

4.2. Class-conditional generation

We evaluate the four-plane factorized latent space in a variety of generative settings, starting with class-conditional generation. Our evaluation is on the same two autoencoders described in the previous section, trained on K600 for 17 frame video reconstruction, at 128×128 and 256×256 resolutions. For generation, we train a transformer-based diffusion model to generate factorized latent embeddings, following Section 3.2. The diffusion model is trained on the UCF-101 dataset [47], which comprises 9,537 videos spanning 101 action categories, offering a diverse set of motion dynamics. To evaluate the quality of generated videos, we

Res.	Method	PSNR↑	SSIM↑	LPIPS↓	Seq.Len
128	Volumetric	27.64	0.85	0.049	1280
	4Plane	27.11	0.82	0.051	672
	Volumetric-VAE	27.32	0.84	0.053	1280
	4Plane-VAE	27.03	0.82	0.055	672
256	Volumetric	26.27	0.79	0.089	1280
	4Plane	25.67	0.77	0.104	672
	WF-VAE	27.86	0.83	0.064	1280
	4Plane-WF-VAE	26.98	0.81	0.073	672

Table 1. **Video reconstruction.** We show reconstruction metrics for our four-plane model and the volumetric baseline (W.A.L.T. [19]) on the Kinetics-600 test set, alongside the corresponding sequence length induced by each latent representation. We evaluate tokenizers trained using both autoencoder and VAE frameworks.

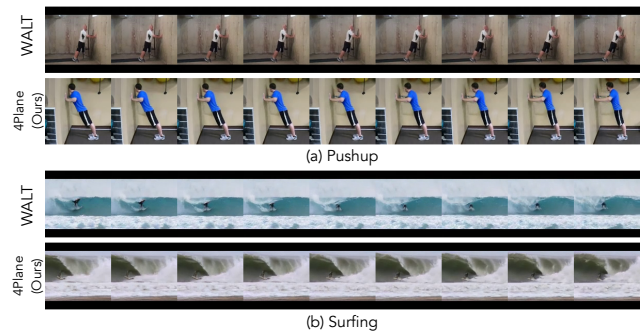


Figure 3. **Class-conditional generation results on the UCF dataset.** We show every other frame of the 17-frame generated videos from the 128×128 models. The temporal continuity and overall frame quality of our factorized model is comparable to the volumetric W.A.L.T. generations.

use the Fréchet Video Distance (FVD) [48] as our primary metric. FVD measures the similarity between the distributions of generated and real videos, assessing both spatial realism and temporal coherence.

4.2.1. Diffusion training details

For a fair comparison, we use a network architecture identical to W.A.L.T. Despite the architecture similarity, W.A.L.T. requires 1.6×10^{12} FLOPs whereas our model only uses 8.5×10^{11} due to shorter sequence lengths. We use a self-conditioning [8] rate of 0.9, AdaLN-LoRA [19] with $r = 2$ as the conditioning mechanism and zero terminal SNR [36] to avoid mismatch between training and inference arising from non-zero signal-to-noise ratio at the final time in noise schedules. We additionally use query-key normalization in the transformer to stabilize training. Our model is trained with a batch size of 256 using an Adam optimizer with a base learning rate of 5×10^{-4} with a linear

	Class Conditional Generation (FVD \downarrow)		Frame Prediction (FVD \downarrow)	Params	Steps
	UCF-101 (128x128)	UCF-101 (256x256)			
Video Diffusion [23]	-	-	16.2	1.1B	256
RIN [26]	-	-	10.7	411M	1000
Phenaki [51]	-	-	36.4	227M	1024
MAGVIT [56]	76	-	9.9	306M	48
PVDM [60]	-	399.4	-	-	400
MAGVIT-v2 [58]	58	-	4.3	307M	24
HVDM [30]	-	303.1	-	63M	100
WALT [19]	46	-	3.3	313M	50
WALT*	39	84.68	5.7	214M	50
4Plane (Ours)	38	58.27	8.6	214M	50

Table 2. **Class-conditional generation on UCF and frame prediction on Kinetics-600.** WALT* represents our re-training and re-evaluation of the WALT baseline. UCF-128 and UCF-256 refer to experiments at 128 x 128 and 256 x 256 resolutions respectively. Our method achieves competitive performance with WALT on the UCF-128 task and performs slightly lower on the K600 frame prediction task, showcasing efficient performance across both datasets. On UCF-256 our model outperforms the baselines.

Type	Method	Davis-7				UCF-7			
		PSNR \uparrow	SSIM \uparrow	LPIPS \downarrow	FVD \downarrow	PSNR \uparrow	SSIM \uparrow	LPIPS \downarrow	FVD \downarrow
Flow Based	AMT [33]	21.09	0.544	0.254	234.5	26.06	0.813	0.144	344.5
	RIFE [25]	20.48	0.511	0.258	240.0	25.73	0.804	0.135	323.8
	FILM [40]	20.71	0.528	0.270	214.8	25.90	0.811	0.137	328.2
Diffusion	LDMVFI [11]	19.98	0.479	0.276	245.0	25.57	0.800	0.135	316.3
	VIDIM [28]	19.62	0.470	0.257	199.3	24.07	0.781	0.149	278.0
	4Plane (Ours)	19.47	0.446	0.256	156.1	24.00	0.769	0.141	216.9

Table 3. **Video interpolation results on DAVIS-7 and UCF-7.** Our method is compared against several video interpolation baselines, assessing both reconstruction and generative metrics, across all 7 interpolated frames. See the text for additional discussion.

warmup and cosine decay.

4.2.2. Analysis

At a resolution of 128×128 , our factorized model outperforms most prior works and performs comparably to W.A.L.T. [19] (see Tab. 2). Furthermore, our model achieves a higher Inception Score of 92.21, compared to 90.95 reported by W.A.L.T. Additionally, the smaller sequence length for our method makes diffusion training and inference nearly 2x faster compared to W.A.L.T. – under identical training architecture and computational resources, our model processes each training iteration in just 380 ms compared to 750 milliseconds for W.A.L.T. We show a detailed timing analysis in the appendix. A comparison of qualitative results are provided in Sec. 4.2.

At 256×256 resolution, our factorization enables a diffusion model that outperforms prior baselines, despite the significant compression. Recall that the factorized sequence length for our 256×256 resolution model is the same as for

128×128 , resulting in 4x more compression. Nonetheless, the generation quality decays relatively much less. Moreover, the comparison to WALT* indicates that a shortened sequence that retains critical spatiotemporal information can in fact reduce the modeling burden on the denoiser network, thereby improving generation quality. We show qualitative comparison in the appendix.

Compared to the tri-plane factorization approaches PVDM [60] and HVDM [30], the four-plane factorization yields substantial improvements, validating the critical design choices of our model. An additional tri-plane ablation is provided in the appendix. Another concern is that the tri-plane structure introduces information mixing in the spatial planes, making the representation unsuitable for different tasks like frame prediction, which we evaluate next.

4.3. Future frame prediction

For the future frame prediction task, we reuse the autoencoder trained for class-conditional generation (Section 4.2).

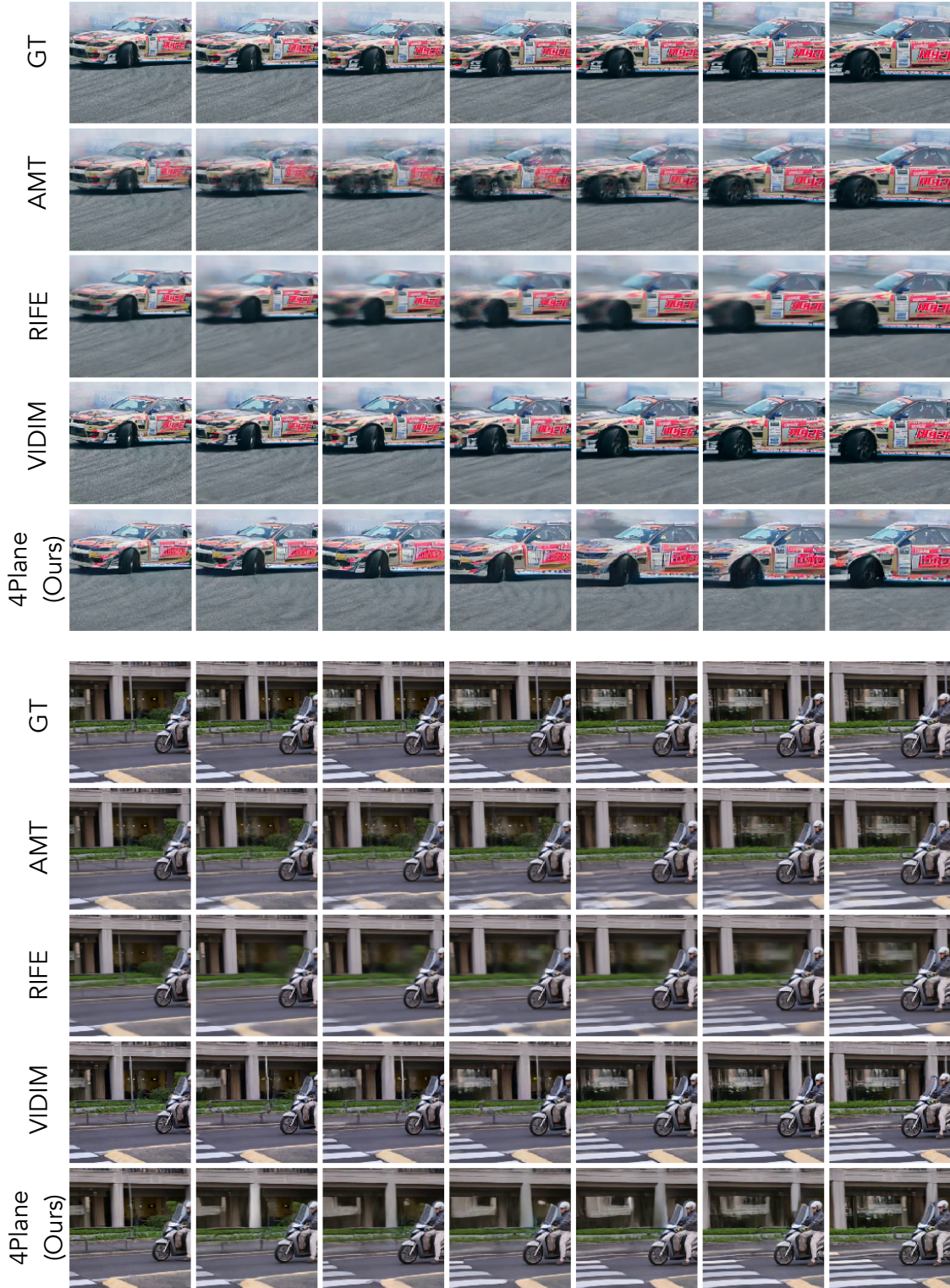


Figure 4. **Interpolation results.** We show the 7 interpolated frames for two scenes from the DAVIS-7 [27] dataset, our method generates realistic videos with sharp, detailed frames, achieving quality comparable to VIDIM [27].

The denoiser network architecture and training procedure remain consistent with the details provided in Sec. 4.2.1, with the key difference that it is trained on K600 to align with the benchmark setting.. The diffusion model uses the first spatial plane \mathbf{P}_{xy}^1 as a conditioning sequence and learns to generate the remaining three planes \mathbf{P}_{xy}^2 , \mathbf{P}_{xt} , and \mathbf{P}_{yt} . By leveraging a causal encoder, this setup mirrors W.A.L.T.’s frame prediction approach, where the model conditions on two latent frames. The frame prediction results in Tab. 2 indicate our model outperforms most prior works and is comparable to WALT* while being significantly faster (see timing analysis in appendix).

4.4. Video interpolation

Video interpolation techniques generate intermediate frames between given keyframes, and are essential for applications requiring fluid motion reconstruction, such as frame-rate upsampling and video inpainting. In this experiment, we leverage our factorized latent representation to train the diffusion model to generate the spatio-temporal plane latents, \mathbf{P}_{xt} and \mathbf{P}_{yt} , conditioned on the spatial plane latents, \mathbf{P}_{xy}^1 and \mathbf{P}_{xy}^2 .

We train our video autoencoder and diffusion model on an internal dataset to encode and generate 256×256 resolution videos with 9 frames. The training and architectural setup closely follow the details outlined in Section 4.2.1. We test on the DAVIS-7 and UCF-7 datasets, as proposed in VIDIM [27]. These datasets consist of 400 videos, each containing 9 frames, and feature scenes with significant and often ambiguous motion.

Table 3 shows the evaluations using reconstruction-based metrics such as PSNR, SSIM, and LPIPS. Although these metrics are commonly used, they can penalize alternative, yet plausible, interpolations. To address this limitation, we also report FVD on the entire video, providing a more holistic evaluation of interpolation quality. We observe that our method performs comparably to VIDIM on the reconstruction metrics. Notably, unlike VIDIM—a diffusion-based baseline requiring a two-stage process with an initial base model followed by a super-resolution step—our model achieves 256×256 resolution video generation in a single stage, making it both simpler and more efficient. We present qualitative results on two DAVIS scenes in Figure 4 to illustrate the effectiveness of our approach in video interpolation. Our method demonstrates comparable quality to the state-of-the-art VIDIM model while producing noticeably sharper details than other methods. These results emphasize the strength of our factorized representation in preserving fine textures and achieving high-fidelity frame generation in complex scenes.

	Factorization Method	FVD \downarrow	Inception \uparrow
UCF-101	Mean Pooling	38	91.13
	Linear Projection	50	89.80
K600	Mean Pooling	8.6	-
	Linear Projection	8.9	-

Table 4. **Factorization method.** We contrast *mean pooling* with *linear projection* for factorizing the volumetric latents.

4.5. Ablation studies

To validate our design choices, we conduct ablations on both the factorization and combine methods across the class-conditional and frame prediction tasks, reporting FVD and Inception scores (IS) for the former, and FVD for the latter. We omit IS for frame prediction as it primarily evaluates classifiability and diversity making it unsuitable for the prediction task. See the appendix for additional ablation experiments.

4.5.1. Factorization

We explore two variations of the factorization operation (Sec. 3.1.1). The first approach applies mean pooling (MP) along Λ_h , Λ_w , and Λ_t , effectively reducing dimensionality while preserving essential features. The second employs a learned linear projection (LP) that maps the channel dimension to 1 along the targeted axis. Both methods perform comparably for frame prediction (Tab. 4, K600). However, for class-conditional generation (Tab. 4, UCF-101), MP significantly outperforms LP. We attribute this gap to the autoencoder’s limited generalization, as it is trained on K600. While both methods achieve similar reconstruction results on the K600 test set, with FVD scores of 7.8 (MP) and 8.0 (LP), their performance diverges on UCF, with FVD of 29.5 (MP) versus 37.1 (LP).

4.5.2. Combine

We also assess different choices for the combine operation (Sec. 3.1.2). Specifically, we test two approaches, *concatenation* defined as $\mathbf{V}(x, y, t) = [\mathbf{f}_{xy}^1 || \mathbf{f}_{xy}^2 || \mathbf{f}_{yt} || \mathbf{f}_{xt}^1]$, and *summation* given by $\mathbf{V}(x, y, t) = \mathbf{f}_{xy}^1 + \mathbf{f}_{xy}^2 + \mathbf{f}_{yt} + \mathbf{f}_{xt}^1$. Table 5 shows that concatenation yields better performance across both the class-conditional generation and frame prediction task. This improvement likely stems from its ability to retain more distinct feature information from each plane.

5. Conclusion

In this work, we introduced a factorized latent representation that encodes videos into a four-plane structure, paving the way for more efficient representation of spatiotemporal signals. Coupled with transformer-based diffusion models, our approach enables up to $2\times$ speedup in training and inference over models operating directly on volumetric latent

	Combine Method	FVD↓	Inception
UCF-101	Concat	38	91.13
	Sum	45	90.76
K600	Concat	8.6	-
	Sum	27	-

Table 5. **Combine method.** We contrast *concatenation* with *summation* for recomposing the volume from the factorized latents.

features—without compromising performance. Our experiments validate that this representation achieves results on par with the previous state-of-the-art across diverse tasks, including class-conditional generation, video extrapolation and interpolation. This work presents a simple and effective way to improve the efficiency of models that work with volumetric latent spaces.

References

- [1] Jie An, Songyang Zhang, Harry Yang, Sonal Gupta, Jia-Bin Huang, Jiebo Luo, and Xi Yin. Latent-shift: Latent diffusion with temporal shift for efficient text-to-video generation. *arXiv preprint arXiv:2304.08477*, 2023. [1](#)
- [2] Omer Bar-Tal, Hila Chefer, Omer Tov, Charles Hermann, Roni Paiss, Shiran Zada, Ariel Ephrat, Junhwa Hur, Guanghui Liu, Amit Raj, et al. Lumiere: A space-time diffusion model for video generation. *arXiv preprint arXiv:2401.12945*, 2024. [2](#)
- [3] Andreas Blattmann, Tim Dockhorn, Sumith Kulal, Daniel Mendelevitch, Maciej Kilian, Dominik Lorenz, Yam Levi, Zion English, Vikram Voleti, Adam Letts, et al. Stable video diffusion: Scaling latent video diffusion models to large datasets. *arXiv preprint arXiv:2311.15127*, 2023. [1, 2](#)
- [4] Andreas Blattmann, Robin Rombach, Huan Ling, Tim Dockhorn, Seung Wook Kim, Sanja Fidler, and Karsten Kreis. Align your latents: High-resolution video synthesis with latent diffusion models. In *Proceedings of the IEEE/CVF Conference on Computer Vision and Pattern Recognition (CVPR)*, pages 22563–22575, 2023. [2](#)
- [5] Andreas Blattmann, Robin Rombach, Huan Ling, Tim Dockhorn, Seung Wook Kim, Sanja Fidler, and Karsten Kreis. Align your latents: High-resolution video synthesis with latent diffusion models. In *IEEE Conference on Computer Vision and Pattern Recognition (CVPR)*, 2023. [1](#)
- [6] Joao Carreira, Eric Noland, Andras Banki-Horvath, Chloe Hillier, and Andrew Zisserman. A short note about kinetics-600. *arXiv preprint arXiv:1808.01340*, 2018. [5](#)
- [7] Anpei Chen, Zexiang Xu, Andreas Geiger, Jingyi Yu, and Hao Su. Tensorf: Tensorial radiance fields. In *European conference on computer vision*, pages 333–350. Springer, 2022. [2](#)
- [8] Ting Chen, Ruixiang Zhang, and Geoffrey Hinton. Analog bits: Generating discrete data using diffusion models with self-conditioning. *arXiv preprint arXiv:2208.04202*, 2022. [5](#)
- [9] Özgün Çiçek, Ahmed Abdulkadir, Soeren S Lienkamp, Thomas Brox, and Olaf Ronneberger. 3d u-net: learning dense volumetric segmentation from sparse annotation. In *Medical Image Computing and Computer-Assisted Intervention—MICCAI 2016: 19th International Conference, Athens, Greece, October 17–21, 2016, Proceedings, Part II* 19, pages 424–432. Springer, 2016. [2](#)
- [10] Xiaoliang Dai, Ji Hou, Chih-Yao Ma, Sam Tsai, Jialiang Wang, Rui Wang, Peizhao Zhang, Simon Vandenhende, Xiaofang Wang, Abhimanyu Dubey, et al. Emu: Enhancing image generation models using photogenic needles in a haystack. *arXiv preprint arXiv:2309.15807*, 2023. [1, 2](#)
- [11] Duolikun Danier, Fan Zhang, and David Bull. Ldmvfi: Video frame interpolation with latent diffusion models. In *Proceedings of the AAAI Conference on Artificial Intelligence*, pages 1472–1480, 2024. [2, 6](#)
- [12] Prafulla Dhariwal and Alexander Nichol. Diffusion models beat gans on image synthesis. *Advances in neural information processing systems*, 34:8780–8794, 2021. [2](#)
- [13] Jiong Dong, Kaoru Ota, and Mianxiong Dong. Video frame interpolation: A comprehensive survey. *ACM Transactions on Multimedia Computing, Communications and Applications*, 19(2s):1–31, 2023. [2](#)
- [14] Patrick Esser, Robin Rombach, and Bjorn Ommer. Taming transformers for high-resolution image synthesis. In *Proceedings of the IEEE/CVF conference on computer vision and pattern recognition*, pages 12873–12883, 2021. [2](#)
- [15] NVIDIA et. al. Cosmos world foundation model platform for physical ai. *arXiv preprint arXiv:2501.03575*, 2025. [2](#)
- [16] Sara Fridovich-Keil, Giacomo Meanti, Frederik Rahbæk Warburg, Benjamin Recht, and Angjoo Kanazawa. K-planes: Explicit radiance fields in space, time, and appearance. In *Proceedings of the IEEE/CVF Conference on Computer Vision and Pattern Recognition*, pages 12479–12488, 2023. [2](#)
- [17] Rohit Girdhar, Mannat Singh, Andrew Brown, Quentin Duval, Samaneh Azadi, Sai Saketh Rambhatla, Akbar Shah, Xi Yin, Devi Parikh, and Ishan Misra. Emu video: Factorizing text-to-video generation by explicit image conditioning. *arXiv preprint arXiv:2311.10709*, 2023. [1](#)
- [18] Yuwei Guo, Ceyuan Yang, Anyi Rao, Zhengyang Liang, Yaohui Wang, Yu Qiao, Maneesh Agrawala, Dahua Lin, and Bo Dai. Animatediff: Animate your personalized text-to-image diffusion models without specific tuning. *arXiv preprint arXiv:2307.04725*, 2023. [2](#)
- [19] Agrim Gupta, Lijun Yu, Kihyuk Sohn, Xiuye Gu, Meera Hahn, Li Fei-Fei, Irfan Essa, Lu Jiang, and José Lezama. Photorealistic video generation with diffusion models, 2023. [1, 2, 5, 6, 3](#)
- [20] Yingqing He, Tianyu Yang, Yong Zhang, Ying Shan, and Qifeng Chen. Latent video diffusion models for high-fidelity long video generation. 2022. [2](#)
- [21] Jonathan Ho, Ajay Jain, and Pieter Abbeel. Denoising diffusion probabilistic models. *Advances in neural information processing systems*, 33:6840–6851, 2020. [2, 4, 3](#)
- [22] Jonathan Ho, William Chan, Chitwan Saharia, Jay Whang, Ruiqi Gao, Alexey Gritsenko, Diederik P Kingma, Ben Poole, Mohammad Norouzi, David J Fleet, et al. Imagen

video: High definition video generation with diffusion models. *arXiv preprint arXiv:2210.02303*, 2022. 2

[23] Jonathan Ho, Tim Salimans, Alexey Gritsenko, William Chan, Mohammad Norouzi, and David J Fleet. Video diffusion models. *Advances in Neural Information Processing Systems*, 35:8633–8646, 2022. 2, 6

[24] Emiel Hoogeboom, Jonathan Heek, and Tim Salimans. simple diffusion: End-to-end diffusion for high resolution images. In *International Conference on Machine Learning*, pages 13213–13232. PMLR, 2023. 2

[25] Zhewei Huang, Tianyuan Zhang, Wen Heng, Boxin Shi, and Shuchang Zhou. Real-time intermediate flow estimation for video frame interpolation. In *European Conference on Computer Vision*, pages 624–642. Springer, 2022. 6

[26] Allan Jabri, David Fleet, and Ting Chen. Scalable adaptive computation for iterative generation. *arXiv preprint arXiv:2212.11972*, 2022. 6

[27] Siddhant Jain, Daniel Watson, Eric Tabellion, Aleksander Hołyński, Ben Poole, and Janne Kontkanen. Video interpolation with diffusion models. In *CVPR*, 2024. 2, 7, 8

[28] Siddhant Jain, Daniel Watson, Eric Tabellion, Ben Poole, Janne Kontkanen, et al. Video interpolation with diffusion models. In *Proceedings of the IEEE/CVF Conference on Computer Vision and Pattern Recognition*, pages 7341–7351, 2024. 6

[29] Simon Kiehhaber, Simon Niklaus, Feng Liu, and Simone Schaub-Meyer. Benchmarking video frame interpolation. *arXiv preprint arXiv:2403.17128*, 2024. 2

[30] Kihong Kim, Haneol Lee, Jihye Park, Seyeon Kim, Kwanghee Lee, Seungryong Kim, and Jaejun Yoo. Hybrid video diffusion models with 2d triplane and 3d wavelet representation. In *European Conference on Computer Vision*, pages 148–165. Springer, 2024. 6

[31] Diederik P Kingma and Max Welling. Auto-encoding variational bayes. *arXiv preprint arXiv:1312.6114*, 2013. 5

[32] Jumin Lee, Sebin Lee, Changho Jo, Woobin Im, Juhyeong Seon, and Sung-Eui Yoon. Semicity: Semantic scene generation with triplane diffusion. In *CVPR*, 2024. 2

[33] Zhen Li, Zuo-Liang Zhu, Ling-Hao Han, Qibin Hou, Chun-Le Guo, and Ming-Ming Cheng. Amt: All-pairs multi-field transforms for efficient frame interpolation. In *Proceedings of the IEEE/CVF Conference on Computer Vision and Pattern Recognition*, pages 9801–9810, 2023. 6

[34] Zongjian Li, Bin Lin, Yang Ye, Liuhan Chen, Xinhua Cheng, Shenghai Yuan, and Li Yuan. Wf-vae: Enhancing video vae by wavelet-driven energy flow for latent video diffusion model. *arXiv preprint arXiv:2411.17459*, 2024. 5

[35] Bin Lin, Yunyang Ge, Xinhua Cheng, Zongjian Li, Bin Zhu, Shaodong Wang, Xianyi He, Yang Ye, Shenghai Yuan, Liuhan Chen, et al. Open-sora plan: Open-source large video generation model. *arXiv preprint arXiv:2412.00131*, 2024. 5

[36] Shanchuan Lin, Bingchen Liu, Jiashi Li, and Xiao Yang. Common diffusion noise schedules and sample steps are flawed. In *Proceedings of the IEEE/CVF winter conference on applications of computer vision*, pages 5404–5411, 2024. 5

[37] Dustin Podell, Zion English, Kyle Lacey, Andreas Blattmann, Tim Dockhorn, Jonas Müller, Joe Penna, and Robin Rombach. Sdxl: Improving latent diffusion models for high-resolution image synthesis. *arXiv preprint arXiv:2307.01952*, 2023. 1, 2

[38] Adam Polyak, Amit Zohar, Andrew Brown, Andros Tjandra, Animesh Sinha, Ann Lee, Apoorv Vyas, Bowen Shi, Chih-Yao Ma, Ching-Yao Chuang, et al. Movie gen: A cast of media foundation models. *arXiv preprint arXiv:2410.13720*, 2024. 1

[39] Ali Razavi, Aaron Van den Oord, and Oriol Vinyals. Generating diverse high-fidelity images with vq-vae-2. *Advances in neural information processing systems*, 32, 2019. 2

[40] Fitsum Reda, Janne Kontkanen, Eric Tabellion, Deqing Sun, Caroline Pantofaru, and Brian Curless. Film: Frame interpolation for large motion. In *European Conference on Computer Vision*, pages 250–266. Springer, 2022. 6

[41] Robin Rombach, Andreas Blattmann, Dominik Lorenz, Patrick Esser, and Björn Ommer. High-resolution image synthesis with latent diffusion models, 2021, 2021. 1, 3

[42] Olaf Ronneberger, Philipp Fischer, and Thomas Brox. U-net: Convolutional networks for biomedical image segmentation. In *Medical image computing and computer-assisted intervention–MICCAI 2015: 18th international conference, Munich, Germany, October 5–9, 2015, proceedings, part III* 18, pages 234–241. Springer, 2015. 2

[43] Chitwan Saharia, William Chan, Saurabh Saxena, Lala Li, Jay Whang, Emily L Denton, Kamyar Ghasemipour, Raphael Gontijo Lopes, Burcu Karagol Ayan, Tim Salimans, et al. Photorealistic text-to-image diffusion models with deep language understanding. *Advances in neural information processing systems*, 35:36479–36494, 2022. 2

[44] Tim Salimans and Jonathan Ho. Progressive distillation for fast sampling of diffusion models. *arXiv preprint arXiv:2202.00512*, 2022. 4

[45] J. Ryan Shue, Eric Ryan Chan, Ryan Po, Zachary Ankner, Jiajun Wu, and Gordon Wetzstein. 3d neural field generation using triplane diffusion. In *CVPR*, 2023. 2

[46] Jiaming Song, Chenlin Meng, and Stefano Ermon. Denoising diffusion implicit models. *arXiv preprint arXiv:2010.02502*, 2020. 3

[47] K Soomro. Ucf101: A dataset of 101 human actions classes from videos in the wild. *arXiv preprint arXiv:1212.0402*, 2012. 5, 1

[48] Thomas Unterthiner, Sjoerd van Steenkiste, Karol Kurach, Raphaël Marinier, Marcin Michalski, and Sylvain Gelly. Fvd: A new metric for video generation. 2019. 5

[49] Aaron Van Den Oord, Oriol Vinyals, et al. Neural discrete representation learning. *Advances in neural information processing systems*, 30, 2017. 2

[50] Ashish Vaswani, Noam Shazeer, Niki Parmar, Jakob Uszkoreit, Llion Jones, Aidan N Gomez, Łukasz Kaiser, and Illia Polosukhin. Attention is all you need. In *Advances in Neural Information Processing Systems*. Curran Associates, Inc., 2017. 3

[51] Ruben Villegas, Mohammad Babaizadeh, Pieter-Jan Kindermans, Hernan Moraldo, Han Zhang, Mohammad Taghi

Saffar, Santiago Castro, Julius Kunze, and Dumitru Erhan. Phenaki: Variable length video generation from open domain textual descriptions. In *International Conference on Learning Representations*, 2022. 6

[52] Junke Wang, Yi Jiang, Zehuan Yuan, BINGYUE PENG, Zuxuan Wu, and Yu-Gang Jiang. Omnitokenizer: A joint image-video tokenizer for visual generation. In *Advances in Neural Information Processing Systems*, pages 28281–28295. Curran Associates, Inc., 2024. 2, 5

[53] Jay Zhangjie Wu, Yixiao Ge, Xintao Wang, Stan Weixian Lei, Yuchao Gu, Yufei Shi, Wynne Hsu, Ying Shan, Xiaohu Qie, and Mike Zheng Shou. Tune-a-video: One-shot tuning of image diffusion models for text-to-video generation. In *Proceedings of the IEEE/CVF International Conference on Computer Vision*, pages 7623–7633, 2023. 2

[54] Rundi Wu, Ruoshi Liu, Carl Vondrick, and Changxi Zheng. Sin3dm: Learning a diffusion model from a single 3d textured shape. *arXiv preprint arXiv:2305.15399*, 2023. 2

[55] Zhuoyi Yang, Jiayan Teng, Wendi Zheng, Ming Ding, Shiyu Huang, Jiazheng Xu, Yuanming Yang, Wenyi Hong, Xiaohan Zhang, Guanyu Feng, et al. Cogvideox: Text-to-video diffusion models with an expert transformer. *arXiv preprint arXiv:2408.06072*, 2024. 2, 5

[56] Lijun Yu, Yong Cheng, Kihyuk Sohn, José Lezama, Han Zhang, Huiwen Chang, Alexander G Hauptmann, Ming-Hsuan Yang, Yuan Hao, Irfan Essa, et al. Magvit: Masked generative video transformer. In *Proceedings of the IEEE/CVF Conference on Computer Vision and Pattern Recognition*, pages 10459–10469, 2023. 2, 6, 1

[57] Lijun Yu, José Lezama, Nitesh B Gundavarapu, Luca Versari, Kihyuk Sohn, David Minnen, Yong Cheng, Vighnesh Birodkar, Agrim Gupta, Xiuye Gu, et al. Language model beats diffusion–tokenizer is key to visual generation. *arXiv preprint arXiv:2310.05737*, 2023. 2

[58] Lijun Yu, Jose Lezama, Nitesh Bharadwaj Gundavarapu, Luca Versari, Kihyuk Sohn, David Minnen, Yong Cheng, Agrim Gupta, Xiuye Gu, Alexander G Hauptmann, Boqing Gong, Ming-Hsuan Yang, Irfan Essa, David A Ross, and Lu Jiang. Language model beats diffusion - tokenizer is key to visual generation. In *ICLR*, 2024. 3, 6, 1, 2

[59] Sihyun Yu, Kihyuk Sohn, Subin Kim, and Jinwoo Shin. Video probabilistic diffusion models in projected latent space. In *Proceedings of the IEEE/CVF conference on computer vision and pattern recognition*, pages 18456–18466, 2023. 2

[60] Sihyun Yu, Kihyuk Sohn, Subin Kim, and Jinwoo Shin. Video probabilistic diffusion models in projected latent space. In *CVPR*, 2023. 1, 6

[61] Sihyun Yu, Weili Nie, De-An Huang, Boyi Li, Jinwoo Shin, and Anima Anandkumar. Efficient video diffusion models via content-frame motion-latent decomposition. *arXiv preprint arXiv:2403.14148*, 2024. 1

[62] Sijie Zhao, Yong Zhang, Xiaodong Cun, Shaoshu Yang, Muyao Niu, Xiaoyu Li, Wenbo Hu, and Ying Shan. Cv-vae: A compatible video vae for latent generative video models. *Advances in Neural Information Processing Systems*, 37: 12847–12871, 2025. 2, 5

A. Frames vs Reconstruction Quality

We evaluate the performance of the four-plane factorized representation as the number of video frames increases. Specifically, we test videos with 17, 21, and 25 frames, and report reconstruction performance in Table 6. We observe that increasing the number of frames from 17 to 25 has only a minor impact on reconstruction quality.

Frames	PSNR↑	SSIM↑	LPIPS↓
17	27.11	0.82	0.051
21	26.95	0.82	0.051
25	26.51	0.81	0.052

Table 6. **Video reconstruction.** We report reconstruction metric of 4Plane tokenizer for various video lengths.

B. Longer Video Generation

To demonstrate our model’s performance on longer sequences, we extend the class-conditional generation experiments to 36 and 56 frames, with results presented in Tab. 7. For 36 frames, our method achieves comparable performance to WALT while running 5× faster. In the 56-frame setup, WALT exceeds memory limits due to the increased sequence length, whereas our approach remains efficient.

FVD (ms/step)		
	36 frame	56 frames
WALT	164 (1350)	OOM
4Plane (Ours)	171 (270)	564 (378)

Table 7. **Longer Video Generataion.** We report the FVD and training time per step (ms / step) for videos with 36 and 56 frame.

C. Timing details

A detailed timing breakdown for various components of the model during training, measured with different batch sizes on TPU v5e, TPU v4, V100, and A100 devices in the class-conditional generation setting, is provided in Figure 5. These timings were obtained using a model with 214M parameters, alternating between our factorized latent representation and the volumetric latent baseline. For each plot, timings are reported up to the maximum batch size supported on each device. The timings reported in Section 4.2.2 correspond to a model trained on a 4 × 8 TPU v5e architecture with a batch size of 256. These measurements approximately align with the timings for a batch size of 8 shown in row 1 of Figure 5.

Across all devices, our model supports larger batch sizes due to its reduced memory requirements. For instance, on TPU v5e (Figure 5), our model accommodates a batch size of 18, whereas the baseline is limited to 10.

The decoder network incurs slightly higher execution time because it contains nearly twice the parameters of the encoder. Although the encoder and decoder in our model are marginally slower than the baseline autoencoder due to the additional factorization and recomposition operations, these operations are executed only once, compared to the denoiser network which is run for 50 steps during inference, keeping their overall impact minimal.

During inference on a 128 × 128 video with 17 frames, the 4Plane representation takes 0.17 seconds per video, while the volumetric representation takes 0.40 seconds per video, measured on a 2 × 2 TPU v5e.

D. Triplane Ablation

Number of Planes	FVD↓	Inception↑
Four-plane	38	91.13
Tri-plane	52	90.46

Table 8. **Ablation: number of planes.** We report FVD and Inception scores on the class-conditional task for the UCF-101 [47] dataset comparing performance between tri-plane and four plane representation.

To assess the impact of the four-plane representation we perform an experiment where we substitute the four-plane representation with tri-plane. We report the results in Table 8. We only conduct this ablation on the class-conditional task as the frame prediction task cannot be achieved with three plane representation. The superior performance of the four-plane representation over the tri-plane approach can be attributed to its increased capacity for capturing spatial information. By incorporating two spatial planes rather than a single one, the four-plane factorization preserves a more comprehensive set of spatial features, reducing information loss while also providing additional flexibility in its ability to be applied towards frame-conditional tasks in a straightforward manner.

E. Implementation details

E.1. Video autoencoder

To incorporate image data into the training of the video autoencoder, we adopt an image pretraining strategy commonly employed in prior works [19, 56, 58]. Specifically, we first train an image autoencoder using 2D convolutional layers. The trained weights are then used to initialize the video autoencoder. Following the approach in

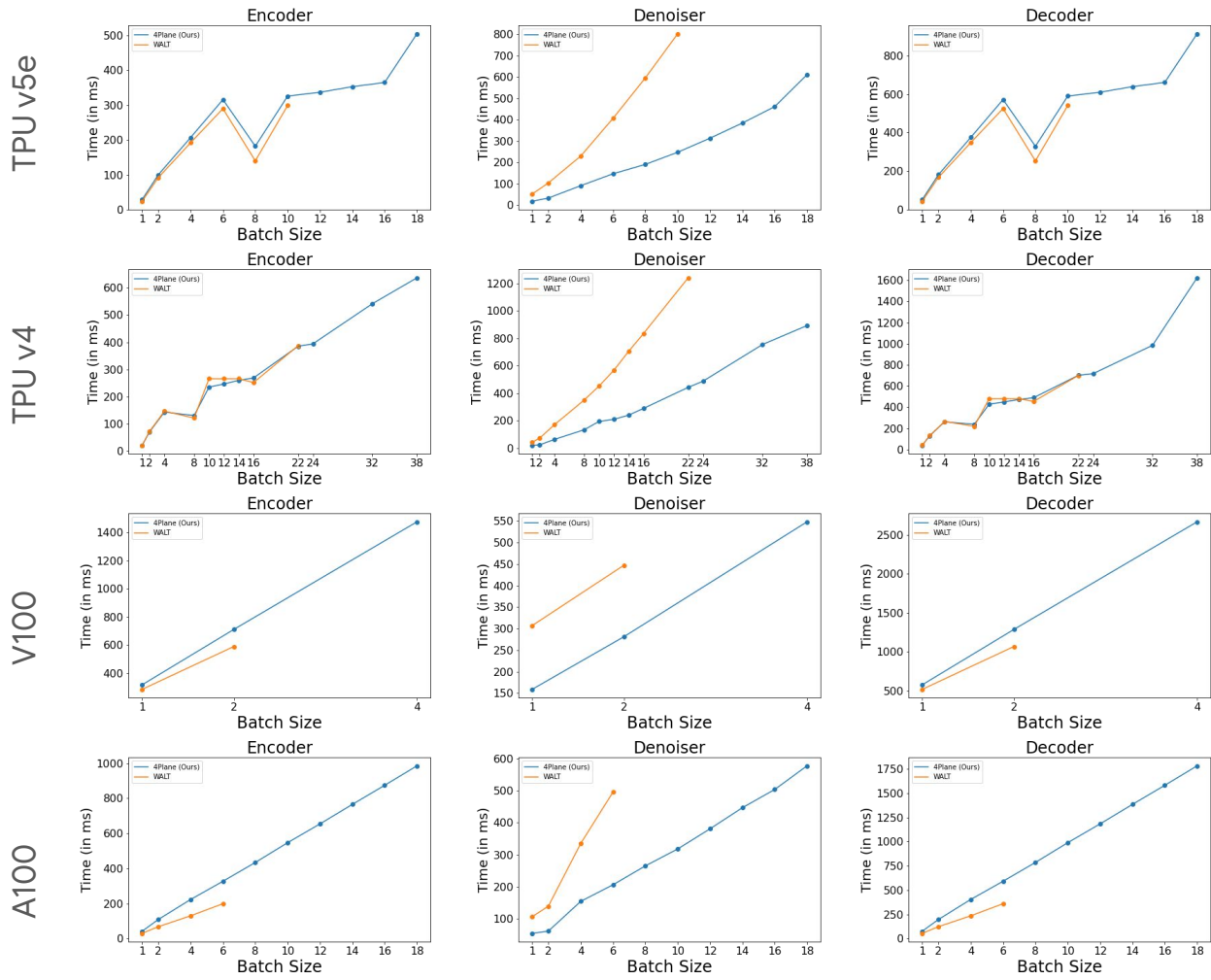


Figure 5. Timing Breakdown. Execution times for the encoder, denoiser, and decoder are reported across varying batch sizes on TPU architectures (v5e and v4) in Rows 1 and 2, and GPU architectures (V100 and A100) in Rows 3 and 4. The comparison includes timings for factorized latents (blue) and volumetric latents (orange), measured up to the maximum batch size supported without running out of memory (OOM) for each configuration. The timings are reported for a single step measured during training.

MAGVITv2 [58], which shares a similar architecture with our model, we inflate the 2D weights to 3D by initializing the 3D filters to zero and assigning the last slice of the 3D filter to the corresponding 2D filter weights. This method ensures a smooth transition from image-based training to video-based learning, leveraging the pre-trained image representations effectively. For the 128×128 experiments, the tokenizer consists of 4 residual blocks in both the encoder and decoder, with 2 temporal downsampling layers and 3 spatial downsampling layers. At 256×256 , we increase the capacity to 5 residual blocks, maintaining 2 temporal downsampling layers while expanding to 4 spatial downsampling

layers. To train the autoencoder we use a combination of objectives, including an L2 reconstruction loss, a perceptual loss, and an adversarial loss, to ensure high-quality latent representations that preserve both fine details and overall structure. For the VAE experiments in Section 4.1, we add an additional KL loss with a weight of 10^{-6}

For class conditional and frame prediction task, we train the tokenizer for 270,000 iterations with a batch size of 256. The resulting autoencoder achieves a reconstruction performance of 27.11 PSNR and 0.829 SSIM on videos with 128×128 resolution and 17 frames.

For the video interpolation task, the autoencoder is

trained for 450,000 iterations with the same batch size of 256. It achieves a reconstruction PSNR of 25.58 and SSIM of 0.717 on videos with 256×256 resolution and 9 temporal frames.

E.2. Denoiser

We use the same transformer architecture across all three tasks, following the design and hyperparameters outlined in W.A.L.T. [19].

- **Class-conditional generation:** The denoiser is trained for 74,000 iterations with a batch size of 256. For the 128×128 resolution experiments, the input sequence has a length of 672, comprising two spatial planes with a resolution of 16×16 each and two spatio-temporal planes with a resolution of 5×16 each. For the 256×256 resolution experiments the dimension of the planes and thus the sequence length remains the same due to the additional temporal downsampling.
- **Frame prediction:** The denoiser is trained for 270,000 iterations with a batch size of 256. The input sequence has a length of 416, composed of one spatial plane with a resolution of 16×16 and two spatio-temporal planes with a resolution of 5×16 each. The conditioning sequence has a length of 256, formed by flattening the first spatial plane, which contains information equivalent to the first two latent frames used as conditioning in W.A.L.T.
- **Video interpolation:** The model is trained for 100,000 iterations with a batch size of 256. The target sequence has a length of 96, corresponding to the two spatio-temporal planes, while the conditioning sequence has a length of 512.

E.3. Diffusion

During training, we adopt a scaled linear noise schedule [41] with $\beta_0 = 0.0001$ and $\beta_T = 0.002$, utilizing a DDPM sampler [21] for the forward diffusion process. During inference, we switch to a DDIM sampler [46] with 50 steps.

F. Joint Image Video Training

While we have not experimented with it, our four-plane representation can be applied in the joint image-video training setting using the following strategy. When encoding a single image with our 4Plane encoder, the output consists of two identical spatial planes and two spatio-temporal vectors. One of the redundant spatial planes can be discarded, allowing us to use the remaining spatial plane along with the spatio-temporal vectors to train the denoiser network. This results in a slight increase in sequence length compared to the volumetric baseline. For example, given a latent grid of size $1 \times 16 \times 16$, the sequence length increases from 256 (volumetric) to 288 (4Plane), due to the inclusion of two additional spatio-temporal vectors of size 16 each. This

strategy allows for using the same autoencoder and denoiser network for images and videos.